# Pairing and continuum effects in nuclei close to the drip line

M. Grasso,[1] N. Sandulescu,[2] Nguyen Van Giai,[1] and R. J. Liotta[3]
[1]*Institut de Physique Nucléaire, IN2P3-CNRS, Université Paris-Sud, F-91406 Orsay Cedex, France*
[2]*Institute for Physics and Nuclear Engineering, P.O. Box MG-6, 76900 Bucharest, Romania*
[3]*Royal Institute of Technology, Frescativagen 24, S-10405 Stockholm, Sweden*
(Received 22 June 2001; published 21 November 2001)

The Hartree-Fock-Bogoliubov (HFB) equations in coordinate representation are solved exactly, i.e., with correct asymptotic boundary conditions for the continuous spectrum. The calculations are performed with effective Skyrme interactions. The exact HFB solutions are compared with HFB calculations based on box boundary conditions and with resonant continuum Hartree-Fock-BCS (HF-BCS) results. The comparison is done for the neutron-rich Ni isotopes. It is shown that close to the drip line the amount of pairing correlations depends on how the continuum coupling is treated. On the other hand, the resonant continuum HF-BCS results are generally close to those of HFB even in neutron-rich nuclei.

DOI: 10.1103/PhysRevC.64.064321 PACS number(s): 21.60.Jz, 27.50.+e

## I. INTRODUCTION

The physics of exotic nuclei close to the drip lines has triggered a new interest for the study of pairing correlations in finite systems. A peculiarity of pairing correlations in weakly bound nuclei is their sensitivity to the effects of unbound single-particle states.

The pairing correlations in the presence of continuum coupling have been treated both in Hartree-Fock-Bogoliubov (HFB) [1–8] and Hartree-Fock-BCS (HF-BCS) [9–12] approximations. In the HFB approximation the continuum is generally included in spherical systems by solving the HFB equations in coordinate representation. The calculations are done either in the complex energy plane by using Green function techniques [1,6], or on the real energy axis [3,4]. In the latter case the HFB equations are usually solved by imposing box boundary conditions, i.e., the HFB wave functions are assumed to vanish beyond some distance that is chosen to be typically a few times the nuclear radius.

The effect of the resonant continuum upon pairing correlations was also studied in the framework of the BCS approximation, both for zero [9–11] and finite temperature [12].

For deformed systems working in coordinate representation is much more difficult [5]. In most of the deformed HFB calculations the continuum is discretized by expanding the HFB wave functions on a single-particle basis. Usually a harmonic oscillator basis is taken and one can improve the description of physical quantities at large distances such as density tails by performing a local scaling transformation [7,8].

The aim of this paper is to show how the coordinate space HFB equations can be actually solved in the case of spherical symmetry and Skyrme type forces by treating the continuum exactly, i.e., with correct boundary conditions, and to analyze to which extent different approximations, namely, box HFB and resonant continuum HF-BCS calculations, compare with the exact solutions. In this paper we will treat the continuum exactly only for the neutrons of neutron-rich systems for which one expects that the continuum plays an important role close to the drip line. For the protons we will treat the continuum by a box discretization. It will be shown that nuclear properties related to pairing correlations are correctly predicted by discretized continuum methods away from drip line but they deviate appreciably from exact continuum results when one approaches the drip line.

The paper is organized as follows. In Sec. II we give a brief reminder of the HFB equations in coordinate representation. In Sec. III we present the procedure we have used for calculating the continuum HFB solutions and we discuss, in a schematic model, how the quasiparticle resonant states are identified. In Sec. IV we present the continuum HFB calculations for Ni isotopes in comparison with box HFB and resonant HF-BCS calculations. Conclusions are drawn in Sec. V.

## II. HFB EQUATIONS IN COORDINATE REPRESENTATION

The HFB approximation in coordinate representation has been discussed quite extensively in the literature [2–4] and, therefore, we recall here only the basic equations.

The HFB equations in coordinate representation read [3]

$$\int d^3\mathbf{r}' \sum_{\sigma'} \begin{pmatrix} h(\mathbf{r}\sigma,\mathbf{r}'\sigma') & \tilde{h}(\mathbf{r}\sigma,\mathbf{r}'\sigma') \\ \tilde{h}(\mathbf{r}\sigma,\mathbf{r}'\sigma') & -h(\mathbf{r}\sigma,\mathbf{r}'\sigma') \end{pmatrix} \begin{pmatrix} \Phi_1(E,\mathbf{r}'\sigma') \\ \Phi_2(E,\mathbf{r}'\sigma') \end{pmatrix} = \begin{pmatrix} E+\lambda & 0 \\ 0 & E-\lambda \end{pmatrix} \begin{pmatrix} \Phi_1(E,\mathbf{r}\sigma) \\ \Phi_2(E,\mathbf{r}\sigma) \end{pmatrix}, \tag{1}$$

where $\lambda$ is the chemical potential, $h$ and $\tilde{h}$ are the mean field and the pairing field, and $(\Phi_i)$ represents the two-component HFB quasiparticle wave function of energy $E$. The mean-field operator $h$ is a sum of the kinetic energy $T$ and the mean field potential $\Gamma$,

$$h(\mathbf{r}\sigma,\mathbf{r}'\sigma') = T(\mathbf{r},\mathbf{r}')\,\delta_{\sigma\sigma'} + \Gamma(\mathbf{r}\sigma,\mathbf{r}'\sigma'). \tag{2}$$

The mean-field potential $\Gamma$ is expressed in terms of the particle-hole two-body interaction $V$ and the particle density $\rho$ in the following way:

 

$$\Gamma(\mathbf{r}\sigma,\mathbf{r}'\sigma')=\int d^3\mathbf{r_1}d^3\mathbf{r_2}\sum_{\sigma_1\sigma_2}V(\mathbf{r}\sigma,\mathbf{r_1}\sigma_1;\mathbf{r}'\sigma',\mathbf{r_2}\sigma_2)\times\rho(\mathbf{r_2}\sigma_2,\mathbf{r_1}\sigma_1). \quad (3)$$

Similarly the pairing field $\tilde{h}$ is expressed in terms of the pairing interaction $V_{pair}$ and the pairing density $\tilde{\rho}$,

$$\tilde{h}(\mathbf{r}\sigma,\mathbf{r}'\sigma')=\int d^3\mathbf{r_1}d^3\mathbf{r_2}\sum_{\sigma_1\sigma_2}2\sigma'\sigma_2'V_{pair}(\mathbf{r}\sigma,\mathbf{r}'-\sigma';\mathbf{r_1}\sigma_1,\mathbf{r_2}-\sigma_2)\tilde{\rho}(\mathbf{r_1}\sigma_1,\mathbf{r_2}\sigma_2). \quad (4)$$

The particle and pairing densities $\rho$ and $\tilde{\rho}$ are defined by the following expressions:

$$\rho(\mathbf{r}\sigma,\mathbf{r}'\sigma')\equiv\sum_{0<E_n<-\lambda}\Phi_2(E_n,\mathbf{r}\sigma)\Phi_2^*(E_n,\mathbf{r}'\sigma')+\int_{-\lambda}^{E_{cutoff}}dE\Phi_2(E,\mathbf{r}\sigma)\Phi_2^*(E,\mathbf{r}'\sigma'), \quad (5)$$

$$\tilde{\rho}(\mathbf{r}\sigma,\mathbf{r}'\sigma')\equiv\sum_{0<E_n<-\lambda}\Phi_2(E_n,\mathbf{r}\sigma)\Phi_1^*(E_n,\mathbf{r}'\sigma')+\int_{-\lambda}^{E_{cutoff}}dE\Phi_2(E,\mathbf{r}\sigma)\Phi_1^*(E,\mathbf{r}'\sigma'), \quad (6)$$

where the sums are over the discrete quasiparticle states with energies $|E|<-\lambda$, and the integrals are over the continuous quasiparticle states with energies $|E|>-\lambda$. The HFB solutions have the following symmetry with respect to $E$:

$$\Phi_1(-E,\mathbf{r}\sigma)=\Phi_2(E,\mathbf{r}\sigma),$$

$$\Phi_2(-E,\mathbf{r}\sigma)=-\Phi_1(E,\mathbf{r}\sigma). \quad (7)$$

As it appears clearly from Eqs. (5) and (6) we choose to work with the positive energies.

The particle-hole and pairing interactions in Eqs. (3) and (4) are chosen as density-dependent contact interactions, so that the integro-differential HFB equations reduce to coupled differential equations. The zero-range character of the pairing interaction is the reason why one has to adopt an energy cutoff as seen in Eqs. (5) and (6).

In this paper we consider systems with spherical symmetry. In this case the wave functions are readily decomposed into their radial and spin-angular parts [3]

$$\Phi_i(E,\mathbf{r}\sigma)=u_i(Elj,r)\frac{1}{r}y_{lj}^{m_j}(\hat{r},\sigma),i=1,2, \quad (8)$$

where

$$y_{lj}^{m}(\hat{r},\sigma)\equiv Y_{lm_l}(\Theta,\Phi)\chi_{1/2}(m_\sigma)\left|lm_l\frac{1}{2}m_\sigma|jm\right\rangle. \quad (9)$$

In the following we use for the upper and lower components of the radial wave functions the standard notation $u_{lj}(E,r)$ and $v_{lj}(E,r)$.

As we have already mentioned, the HFB equations are usually solved by imposing to the radial wave functions the condition that they vanish beyond a given distance $R$ (box radius). In this case the continuous spectrum is replaced by a set of discrete energies, whose density depends on the box radius. In what follows we discuss how the HFB equations can be solved by keeping the correct asymptotic conditions for the neutron wave functions.

## III. THE TREATMENT OF QUASIPARTICLE CONTINUUM

### A. Asymptotic behaviors

The asymptotic behavior of the HFB wave function is determined by the physical condition that, at large distances the nuclear mean field $\Gamma(r)$ and the pairing field $\Delta(r)$ vanish. This condition requires an effective interaction of finite range and finite-range nonlocality. Outside the range of mean fields the equations for $\Phi_i(E,\mathbf{r}\sigma)$ are decoupled and one can readily find the asymptotic behavior of the physical solutions at infinity [2]. Thus, for a negative chemical potential $\lambda$, i.e., for a bound system, there are two well-separated regions in the quasiparticle spectrum.

Between 0 and $-\lambda$ the quasiparticle spectrum is discrete and both upper and lower components of the radial HFB wave function decay exponentially at infinity. For neutrons this implies that those components have the form

$$u_{lj}(E,r)=Ah_l^{(+)}(i\alpha_1 r),$$

$$v_{lj}(E,r)=Bh_l^{(+)}(i\beta_1 r), \quad (10)$$

where $h_l^{(+)}$ are spherical Haenkel functions, $\alpha_1^2=-(2m/\hbar^2)(\lambda+E)$ and $\beta_1^2=(2m/\hbar^2)(\lambda-E)$. These solutions correspond to the bound quasiparticle spectrum. In this case, the solutions are normalized to unity.

For $E>-\lambda$ the spectrum is continuous and the solutions are

$$u_{lj}(E,r)=C[\cos(\delta_{lj})j_l(\alpha_1 r)-\sin(\delta_{lj})n_l(\alpha_1 r)],$$

$$v_{lj}(E,r)=D_1h_l^{(+)}(i\beta_1 r), \quad (11)$$

where $j_l$ and $n_l$ are spherical Bessel and Neumann functions, respectively, and $\delta_{lj}$ is the phase shift corresponding to the angular momentum $(lj)$. One can see that the upper component of the HFB wave function has the standard form of a scattering state while the lower component is always exponentially decaying at infinity.

The asymptotic form of the wave function should be matched with the inner radial wave function, which for $r\to 0$ can be written as follows:

$$\begin{pmatrix}u_{lj}(E,r)\\ v_{lj}(E,r)\end{pmatrix}=D_2\begin{pmatrix}r^{l+1}\\ 0\end{pmatrix}+D_3\begin{pmatrix}0\\ r^{l+1}\end{pmatrix}, \quad (12)$$

The HFB wave function is normalized to the Dirac $\delta$ function of energy. This condition fixes the constant $C$ to the value

$$C=\sqrt{\frac{1}{\pi}\frac{2m}{\hbar^2\alpha_1}}. \tag{13}$$

The radial wave functions are calculated by integrating the HFB equations outwards starting from the initial conditions (12), and inwards starting from Eq. (10) or Eq. (11) depending on the value of $E$. The solutions are propagated by a modified Numerov method towards the matching point, where the continuity conditions for the wave functions and their derivatives are imposed. These conditions determine the coefficients $D_1$, $D_2$, $D_3$, and the phase shift $\delta$ for a quasiparticle state in the continuum; in the case of a discrete quasiparticle state the continuity conditions and the normalization condition determine the coefficients $A$, $B$, $D_2$, $D_3$, and the energy $E$.

The difficulty of an exact continuum calculation, i.e., with asymptotic solutions given by Eq. (11), is to identify the energy regions where the localization of the wave functions changes quickly with the quasiparticle energy. These are the regions of quasiparticle resonant states.

In HFB the quasiparticle resonant states are of two types. A first type corresponds to the single-particle resonances of the mean field. The low-lying resonances of the mean field located close to the particle threshold are very important in the treatment of pairing correlations of weakly bound nuclei because they become strongly populated by pairing correlations.

A second kind of resonant states is specific to the HFB method and corresponds to the bound single-particle states, which in the absence of pairing correlations have an energy $\epsilon<2\lambda$ . In the presence of the pairing field these bound states are coupled with the continuum single-particle states and, therefore, they acquire a width. The positions and the widths of these HFB resonances are related to the total phase shift, calculated from the matching conditions, as [2]

$$\delta(E)\simeq\delta_0(E)+\mathrm{arctg}\frac{\Gamma}{2(E_R-E)}, \tag{14}$$

where $E_R$ and $\Gamma$ are the energy and the width of the resonant quasiparticle state. The function $\delta_0(E)$ is the phase shift of the upper component of the HFB wave function in the HF limit, i.e., $\tilde{h}=0$. In this limit one has

$$h\Phi_1^0=(E+\lambda)\Phi_1^0. \tag{15}$$

If there is no single-particle resonance close to the energy $E+\lambda$ in the HF limit, then the HF phase shift $\delta_0$ has a slow variation in the quasiparticle energy region. In this case the derivative of the total phase shift has a Breit-Wigner form, which can be used for estimating the position and the width of the quasiparticle resonance.

Thus, in the first step of the calculations we study for each $(l,j)$ channel the behavior of the phase shift and we estimate the energies (widths) of the resonant states from the energies where the derivative of the phase shift is maximum (half of its maximum). Then, we choose for the integration in the energy region of a resonant state an energy grid with a small step. In the calculations presented below the energy step in the region of a resonance is $\Gamma/10$ and the energy cutoff is chosen to be minus the depth of the mean field.

### B. Quasiparticle resonances in a schematic model

In order to illustrate how one can identify the quasiparticle resonances in HFB calculations, we take here a simple model [1,2]. Let us assume that the mean field is given by a square well potential of depth $V_0$ and radius $a$. The pairing field is taken also as a constant inside the same radius $a$ and zero outside. In addition, we suppose that the chemical potential $\lambda$ is given. For such a system the radial HFB equations inside the potential well, i.e., for $r\leqslant a$, are

$$\left(\frac{1}{r}\frac{d^2}{dr^2}r-\frac{l(l+1)}{r^2}+\alpha^2\right)u_{lj}-\gamma^2 v_{lj}=0,$$

$$\left(\frac{1}{r}\frac{d^2}{dr^2}r-\frac{l(l+1)}{r^2}+\beta^2\right)v_{lj}-\gamma^2 u_{lj}=0, \tag{16}$$

where $\alpha^2=(2m/\hbar^2)(\lambda+E+U_0)$, $\beta^2=(2m/\hbar^2)(\lambda-E+U_0)$, $\gamma^2=(2m/\hbar^2)\Delta$, and $U_0=-(V_0+V_{so}\vec{l}\cdot\vec{s})$.

The solutions of Eqs. (16) for any value of the quasiparticle energy are

$$u_{lj}=A_+ j_l(k_+r)+A_- j_l(k_-r),$$

$$v_{lj}=A_+ g_+ j_l(k_+r)+A_- g_- j_l(k_-r), \tag{17}$$

where $j_l$ are spherical Bessel functions, $k_\pm=(2m/\hbar^2)[U_0+\lambda\pm(E^2-\Delta^2)^{1/2}]$ and $g_\pm=[E\pm(E^2-\Delta^2)^{1/2}]/\Delta$.

Outside the potential well the HFB equations are decoupled. In this case the type of solutions depends on the quasiparticle energy. They have the forms given by Eqs. (10) and (11).

In order to simulate the potential corresponding to a heavy nucleus close to the drip line, we take for the model parameters the following values: $V_0=45.35$ MeV, $V_{so}=0.5$ MeV, $a=5.2$ fm, $\Delta=1$ MeV, and $\lambda=-2.0$ MeV.

Here, we discuss only the quasiparticle resonant solutions induced by the bound single-particle states that are specific to the HFB approximation. As a typical example we take the case of $p_{1/2}$ states. In the HF limit, i.e., $\Delta=0$, there are two bound states at energies $\epsilon_1=-32.873$ MeV and $\epsilon_2=-10.698$ MeV. When the pairing field is switched on, these states become quasiparticle resonant states at energies $E_1=30.889$ MeV and $E_2=8.735$ MeV with corresponding widths $\Gamma_1=0.40$ keV and $\Gamma_2=24.38$ keV. These values are obtained by solving the HFB equations in the complex energy plane with outgoing wave boundary conditions. On the real energy axis one should find these two resonances from the phase shift behavior. In Fig. 1 we show the phase shift (top) and its derivative (bottom) in the energy region of the second resonant state. One can see that the derivative of the phase shift is maximum at the resonance energy, and it drops

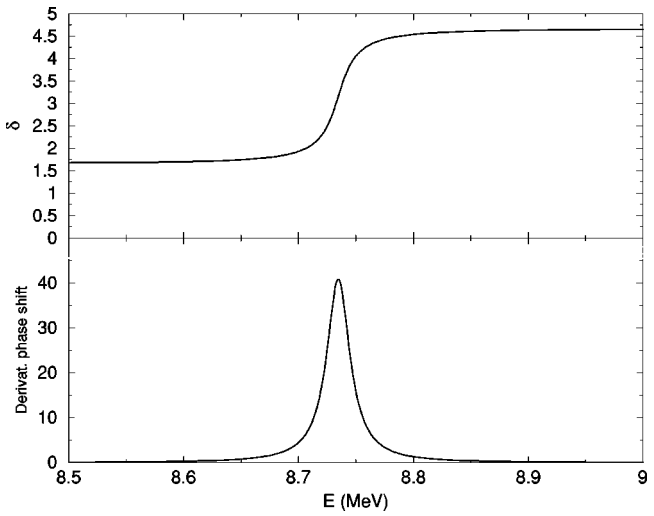


FIG. 1. Phase shift (top) and its derivative (bottom) in the $p_{1/2}$ channel for a square well model.

to half of its maximum value when the energy increases by about 25 keV. This shows that the behavior of the phase shift as a function of the real energy $E$ gives accurate information on the positions and widths of the quasiparticle resonances. From Fig. 1 one can also see that the total phase shift does not cross $\pi/2$ at the resonance energy. As discussed above, the value of the phase shift associated with the resonance energy is actually $\delta_r = \pi/2 + \delta_0$. In this case $\delta_0 = 1.59$, so that the resonance appears when the total phase shift crosses a value close to $\pi$ and not to $\pi/2$. Thus, in order to identify the resonances one can calculate the derivative of the total phase shift and search for the local maxima, or calculate the HF phase shift $\delta_0$ and search for the energies associated to $\delta_r = \pi/2 + \delta_0$. For the $2p_{1/2}$ state analyzed here, the two procedures give exactly the same position of the resonance, but this is not generally the case even for a square well potential [13]. In the present calculations we localize the resonances by using the derivative procedure.

## IV. RESULTS FOR Ni ISOTOPES

In this section we apply the continuum HFB method to the case of Ni isotopes, which have been investigated extensively both in nonrelativistic [5] and relativistic Hartree-Bogoliubov approximation [14,15].

For the Hartree-Fock field we use the Skyrme interaction SIII whereas in the pairing channel we choose a density-dependent zero-range interaction

$$V = V_0 \left[ 1 - \left( \frac{\rho(r)}{\rho_0} \right)^{\gamma} \right] \delta(\mathbf{r}_1 - \mathbf{r}_2), \tag{18}$$

with the following parameters [5]: $V_0 = -1128.75$ MeV, $\rho_0 = 0.134$ fm$^{-3}$, and $\gamma = 1$.

Let us first examine the quasiparticle resonant states for the isotope $^{84}$Ni. After convergence of the self-consistent procedure the chemical potential is $\lambda = -1.104$ MeV. In Table I we show the resonant quasiparticle energies and the widths calculated from the derivatives of the phase shift. The quasiparticle states $2d_{3/2}$, $1g_{7/2}$, and $1h_{11/2}$ originate from single-particle resonances while all the others are related to bound states.

TABLE I. Hartree-Fock single-particle energies $\epsilon$, HFB quasiparticle resonance energies ($E$), and widths ($\Gamma$) in the nucleus $^{84}$Ni, for the various ($lj$) states involved.

| l | $j$ | $\epsilon$ (MeV) | $E$ (MeV) | $\Gamma$ (keV) |
|---|---|---|---|---|
| 0 | 1/2 | -0.731 | 1.276 | |
| | | -22.530 | 20.878 | 98 |
| | | -45.010 | 43.3917 | 0.3 |
| 1 | 1/2 | -9.540 | 7.965 | 338 |
| | | -34.709 | 33.444 | 102 |
| 1 | 3/2 | -11.194 | 9.712 | 576 |
| | | -36.364 | 34.976 | 76 |
| 2 | 3/2 | 0.475 | 2.317 | 816 |
| | | -23.055 | 22.028 | 58 |
| 2 | 5/2 | -1.467 | 1.845 | 44 |
| | | -26.961 | 25.628 | 3 |
| 3 | 5/2 | -10.586 | 8.863 | 944 |
| 3 | 7/2 | -17.023 | 15.857 | 882 |
| 4 | 7/2 | 1.604 | 3.598 | 24 |
| 4 | 9/2 | -6.837 | 5.674 | 3 |
| 5 | 11/2 | 3.295 | 5.380 | 52 |

As already discussed in the case of the schematic model, the positions of some resonances may appear for values of the total phase shifts that are quite far from $\pi/2$. We take here as an example the quasiparticle resonance state corresponding to the bound state $2p_{1/2}$, which was also analyzed in the schematic model. The resonance energy and the width estimated from the derivative of the phase shift are $E = 7.965$ MeV and $\Gamma = 338$ keV. The value of the HF phase shift is in this case $\delta_0 = 0.656$ so that the total phase shift associated with the resonance should be $\delta_r \simeq \pi/2 + 0.656$. The energy corresponding to this phase shift is $E = 7.707$ MeV, which is smaller than the corresponding value extracted from the maximum of the derivative of the phase shift. This shows that in this case the HF phase shift has a non-negligible variation in the energy region of the resonance. However, in practical HFB calculations a small shift in the actual position of a resonance induced by the variation of $\delta_0$ is not essential because this information is used only to fix an appropriate energy grid for the energy integration.

A special behavior can be noticed for the resonant continuum in the $s_{1/2}$ channel. As can be seen in Fig. 2, the occupancy in this channel increases starting from $-\lambda$ up to an energy equal to 1.276 MeV. Therefore, in this channel one needs to use a very small energy step close to $-\lambda$ in order to

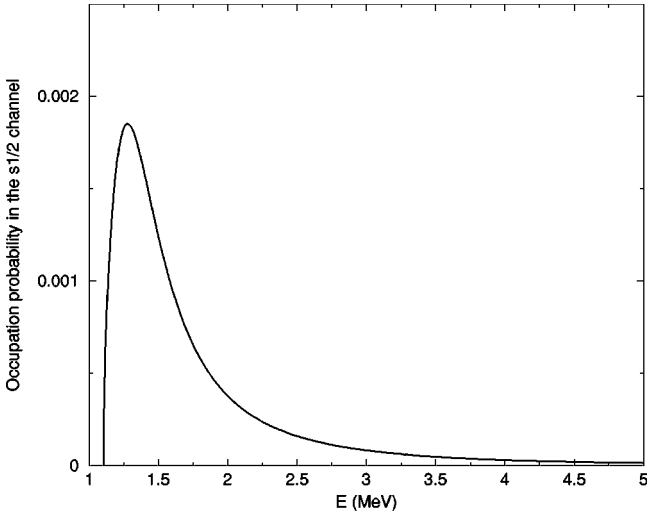


FIG. 2. Occupation probability profile in the $s_{1/2}$ channel for $^{84}$Ni.

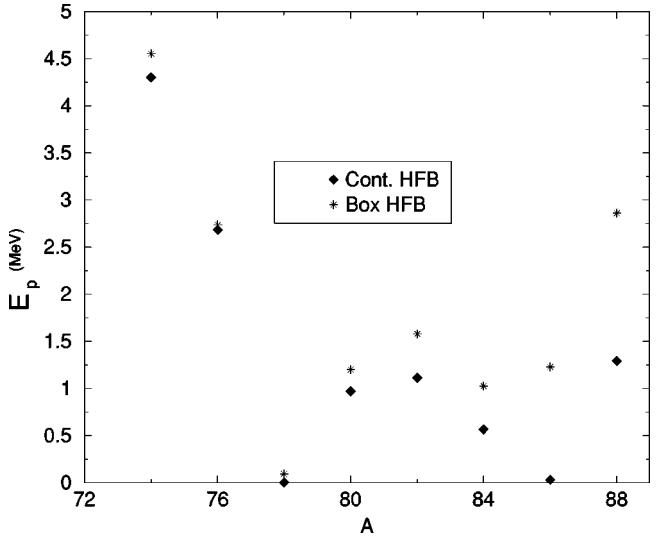


FIG. 3. Pairing correlation energies for Ni isotopes calculated in HFB approximation.

get a correct description of the pairing correlations. Finally one should stress upon the fact that the contribution to the pairing correlations of this pronounced resonant structure close to the quasiparticle continuum threshold is just the manifestation of the loosely bound single-particle state $3s_{1/2}$, which in the HFB approach is embedded in the continuum. This structure has nothing to do with the contribution of the $s_{1/2}$ single-particle background continuum close to zero energy, which remains very small.

### A. Comparison between continuum and box HFB calculations

In this section we analyze the sensitivity of the HFB results to the continuum treatment in the vicinity of a drip line, by comparing the results provided by continuum and box HFB calculations for the chain of neutron-rich Ni isotopes. The energy cutoff is the same in both calculations. For all box calculations presented below the box radius is taken equal to 22.5 fermi. Recently, some box calculations have been reported for carbon isotopes with box radii up to 400 fermi [16]. If these large box HFB codes could also be used for heavier nuclei such as the Ni isotopes the differences that we show here between box and exact results near the drip line might be somewhat reduced.

Lets us first discuss the properties directly related to the pairing correlations, i.e., pairing correlation energies and pairing densities.

The pairing correlation energies are estimated by the difference between the total energies calculated in HFB and HF approach

$$E_p = E(\mathrm{HF}) - E(\mathrm{HFB}). \tag{19}$$

The results for continuum and box HFB calculations are shown in Fig. 3 for all Ni isotopes starting from $A=74$ up to $A=88$, which is the last nucleus with positive two-neutron separation energy, as predicted by the continuum HFB calculations (see below). Up to $^{86}$Ni the quantity $E(\mathrm{HF})$ does not depend on the continuous single-particle spectrum. The isotope $^{88}$Ni is not bound in HF and, therefore, the $E(\mathrm{HF})$ used for estimating the pairing correlation energy is calculated by using a box, as in box HFB calculations. From Fig. 3 one can see that the box HFB calculations start to overestimate the amount of pairing correlations in the proximity of the drip line. Thus, in box calculations the pairing energy for $^{84}$Ni is about twice that of continuum HFB and it is still increasing for $^{86}$Ni, where the continuum HFB calculations predict zero pairing correlation energy.

These differences are reflected in the pairing densities, as shown in Fig. 4 for the isotopes $^{84}$Ni and $^{86}$Ni. One can notice that the box calculations overestimate the pairing correlations in the surface region, where the localization of the resonance wave functions with high $(lj)$ increases. Thus, in the box calculations the resonant states with high $(lj)$ located above the Fermi level are more strongly populated than the corresponding states calculated by using continuum HFB

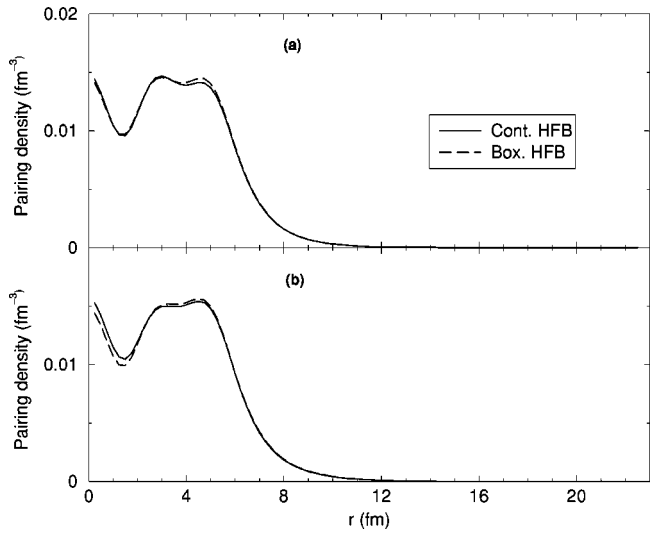


FIG. 4. Neutron pairing densities in HFB calculations in $^{84}$Ni (a) and $^{86}$Ni (b).

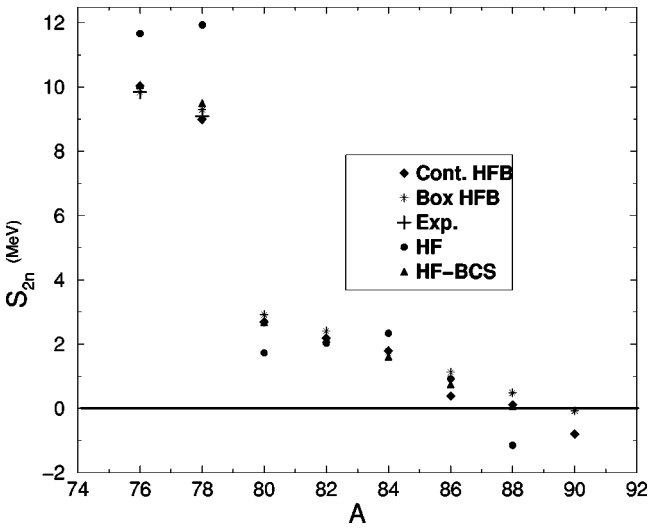


FIG. 5. Two-neutron separation energies in HFB, HF-BCS, and HF approximations. For $^{76}$Ni and $^{78}$Ni the corresponding values extrapolated from experimental data [18] are also shown.

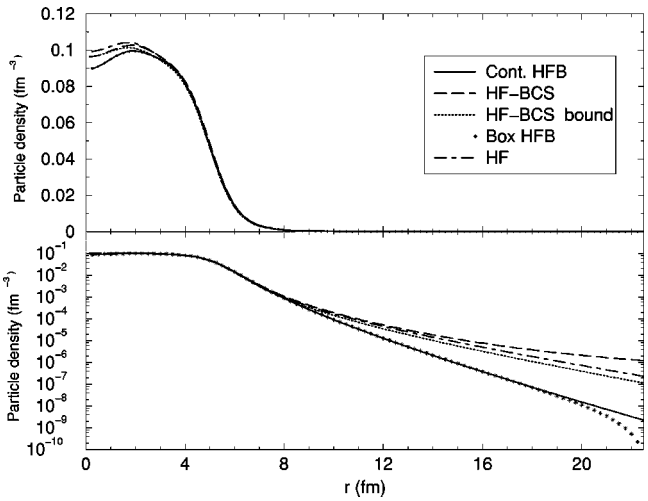


FIG. 6. Neutron particle densities in HFB, resonant continuum HF-BCS, and HF approximations for $^{86}$Ni. The density represented by the dotted line (HF-BCS bound) is calculated by including only the contribution of bound states.

calculations. As an illustration we consider the occupancy of the single-particle resonance $g_{7/2}$. In $^{84}$Ni this resonance is located at 3.6 MeV and has a width of about 25 keV. If we take an energy interval 3.2 MeV$\leqslant E \leqslant$4 MeV around the resonance, we find that the total occupancy of the states in the box that are within this interval is about 2% higher than the corresponding occupancy in the continuum calculations. In box calculations the role of a resonant state is usually taken by one state with an energy close to the energy of the resonance, and this state has maximum localization inside the nucleus. Thus, while in box calculations the pairs can virtually scatter mainly to that state with maximum localization, in continuum HFB calculation the pairs can also scatter to the neighboring states whose wave functions are less concentrated inside the nucleus. As a result the occupancy of a resonance in continuum HFB is smaller. This effect, induced by the width of resonant states, is missing in box HFB calculations.

Let us consider now the two-neutron separation energies $S_{2n}$,

$$S_{2n}=E(Z,N)-E(Z,N-2), \tag{20}$$

which are plotted in Fig. 5. One can see that in both calculations the change of the sign of the two-neutron separation energies, i.e., the position of the two-neutron drip line, is between $^{88}$Ni and $^{90}$Ni, with a faster drop in the case of continuum HFB. The values of $S_{2n}$, evaluated within the two HFB calculations are in better agreement one with the other than the corresponding values of the pairing correlation energies. This is because the differences observed in the pairing correlation energies are much reduced when one calculates the differences appearing in $S_{2n}$. For the same reason one can see that even a HF calculation gives quite resonable values for the two-neutron separation energies close to the drip line. The largest differences between HFB and HF calculations appear across the doubly magic isotope $^{78}$Ni. In this case the pairing energy changes quickly when two neutrons are removed from $1g_{9/2}$ or added to $2d_{5/2}$. Because the hole state has larger degeneracy than the particle state, the pairing correlations are stronger in $^{76}$Ni than in $^{80}$Ni. This explains the asymmetry seen in the behavior of $S_{2n}$ across the doubly magic nucleus $^{78}$Ni. The fact that the value of $S_{2n}$ predicted by HFB for $^{76-78}$Ni is close to the data extrapolated from lighter isotopes indicates that the pairing interaction used in the calculations is quite reasonable, at least for the valence shell $N=28-50$.

Next, we compare the results given by the two HFB calculations for observables related to mean-field properties. In Fig. 6 the particle density for the isotope $^{86}$Ni is shown. One notices that the particle densities are practically the same except in the region near the box radius. The fact that the two-particle densities are very close up to very large distances implies that the neutron root-mean-square (rms) radii calculated within the two approaches should be similar. This can be seen in Fig. 7 for the isotopes $^{80-90}$Ni.

In Fig. 7 the HF radii are also shown. In $^{84}$Ni we can see that the HFB radius is slightly larger than the HF value, which is the trend usually expected when the pairing interaction is switched on. In this case the HFB radius is increased because the pairing interaction scatters some neutrons from $2d_{5/2}$ to the loosely bound state $3s_{1/2}$ which is a state less localized inside the nucleus. On the other hand, as seen in Fig. 7, the effect of pairing correlations on the radius of $^{86}$Ni is opposite. Here, the pairing interaction scatters particles out of $3s_{1/2}$ state that is completely occupied in HF. The particles are scattered in the continuum single-particle states, mainly to single-particle resonances that have a larger localization inside the nucleus than the $3s_{1/2}$ state. Thus, in this case the radius is decreased when the pairing correlations are switched on. This effect of the pairing interaction on nuclear radii is sometimes called ''antihalo'' [6,17].

### B. Comparison between HFB and HF-BCS approximation

The HF-BCS approximation is obtained by neglecting in the HFB equations the non-diagonal matrix elements of the

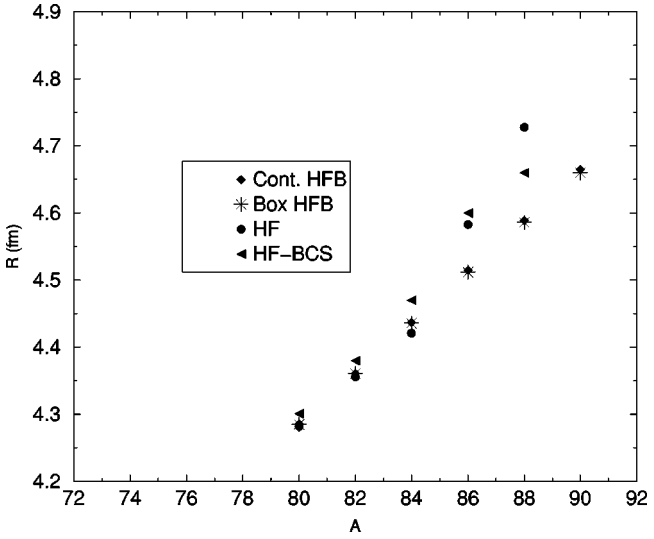


FIG. 7. Neutron rms for Ni isotopes in HFB, resonant continuum HF-BCS, and HF approximations.

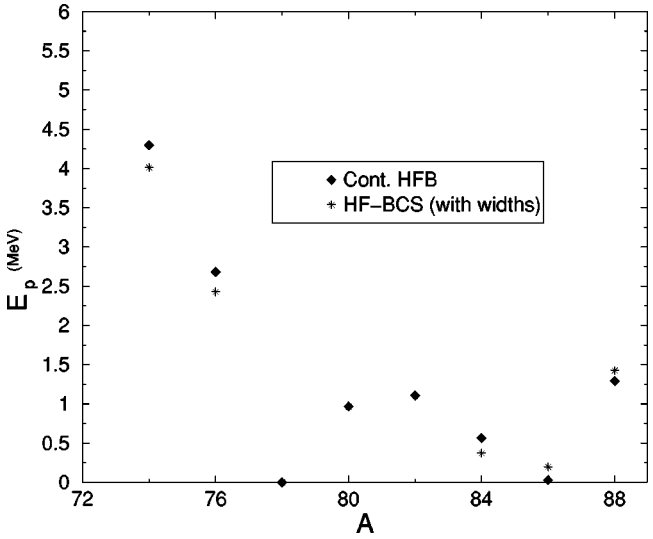


FIG. 8. Pairing correlation energies calculated in resonant continuum HF-BCS approximation compared to continuum HFB.

pairing field. This means that in the HF-BCS limit one neglects the pairing correlations induced by the pairs formed in states that are not time-reversed partners.

The extension of BCS equations for taking into account the continuum coupling was proposed in Refs. [9,10,12]. For the case of a general pairing interaction the BCS equations read [10]

$$\Delta_i = \sum_j V_{i\bar{i}j\bar{j}} u_j v_j + \sum_\nu V_{i\bar{i},\nu\epsilon_\nu\overline{\nu\epsilon_\nu}} \int_{I_\nu} g_\nu(\epsilon) u_\nu(\epsilon) v_\nu(\epsilon) d\epsilon, \tag{21}$$

$$\Delta_\nu \equiv \sum_j V_{\nu\epsilon_\nu\overline{\nu\epsilon_\nu}j\bar{j}} u_j v_j + \sum_{\nu'} V_{\nu\epsilon_\nu\overline{\nu\epsilon_\nu},\nu'\epsilon_{\nu'}\overline{\nu'\epsilon_{\nu'}}} \int_{I_{\nu'}} g_{\nu'}(\epsilon') u_{\nu'}(\epsilon') v_{\nu'}(\epsilon') d\epsilon', \tag{22}$$

$$N = \sum_i v_i^2 + \sum_\nu \int_{I_\nu} g_\nu(\epsilon) v_\nu^2(\epsilon) d\epsilon. \tag{23}$$

Here $\Delta_i$ is the gap for the bound state $i$ and $\Delta_\nu$ is the averaged gap for the resonant state $\nu$. The quantity $g_\nu(\epsilon) = [(2j_\nu+1)/\pi][(d\delta_\nu)/d\epsilon]$ is the continuum level density and $\delta_\nu$ is the phase shift of angular momentum $(l_\nu j_\nu)$. The factor $g_\nu(\epsilon)$ takes into account the variation of the localization of scattering states in the energy region of a resonance (i.e., the width effect) and becomes a delta function in the limit of a very narrow width. In these equations the interaction matrix elements are calculated with the scattering wave functions at resonance energies and normalized inside the volume where the pairing interaction is active. The BCS Eqs. (21)–(23) are solved iteratively together with the HF equations. The corresponding equations are called below the resonant continuum HF-BCS equations. For more details see Ref. [10].

In the case of Ni isotopes the effect of the continuum is introduced through the first three low-lying single-particle resonances, i.e., $d_{3/2}$, $g_{7/2}$, and $h_{11/2}$. These resonances form together with the bound states $2d_{5/2}$ and $3s_{1/2}$ the equivalent of the major shell $N=50$–$82$. The energy integrals in BCS equations (21)–(23) are performed for each resonance in an energy interval defined such that $|\epsilon-\epsilon_\nu| \leqslant 2\Gamma_\nu$, where $\epsilon_\nu$ is the energy of the resonance and $\Gamma_\nu$ is its width. In the resonant continuum HF-BCS calculations we use the same interaction as in HFB approach.

In Fig. 8 we show the pairing correlation energies predicted by the resonant continuum HF-BCS approximation in comparison with the continuum HFB results. One can see that the HF-BCS results follow closely the exact HFB values up to the drip line. This shows that in order to estimate the pairing correlations one needs to include from the whole continuum only a few resonant states with their widths properly considered.

In order to see the effect of the widths of resonant states upon pairing, we replace in the resonant continuum HF-BCS equations the continuum level density by delta functions. This means that the resonant state is replaced by a scattering state at the resonance energy, normalized in a volume of radius $R$. For this radius we take the same value as in box HFB calculations, i.e., $R=22.5$ fm. As it can be seen from Fig. 9, the pairing correlations increase when one neglects the widths of the resonances and the results follow closely those of box HFB calculations. Thus, the overestimation of pairing correlations due to the continuum discretization is similar in HF-BCS and HFB calculations.

In Fig. 7 we show also the radii calculated in the resonant continuum HF-BCS approximation. One notices that the HF-BCS radii are closer to the HF values than to the HFB ones. The same behavior is found for the particle densities. This can be seen in Fig. 6 for the case of $^{86}$Ni, which is the last bound nucleus in the HF approximation. From Fig. 6 one can see also that the tail of the density in resonant continuum HF-BCS calculations is mainly given by the particles distrib-

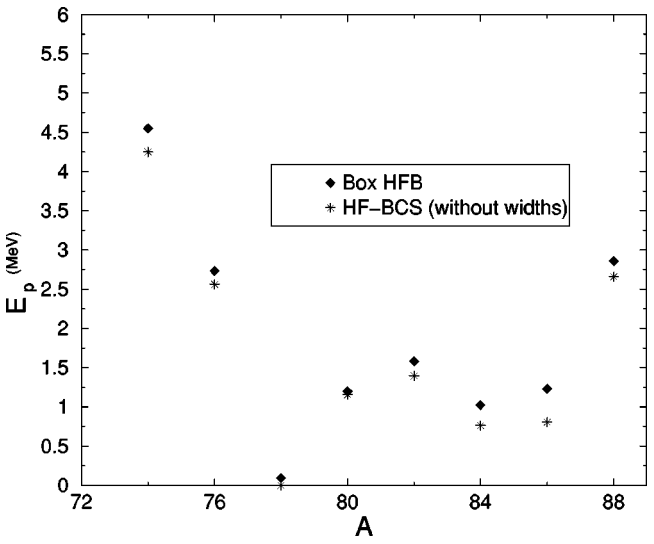


FIG. 9. Pairing correlation energies calculated in the resonant continuum HF-BCS approximation by neglecting the widths effect compared to box HFB results.

uted in the bound states $2d_{5/2}$ and $3s_{1/2}$ and not due to the particles scattered to positive energy states. In HFB calculations a part of the particles from the bound states $2d_{5/2}$ and $3s_{1/2}$ are scattered to other states, mainly to resonant states, with wave functions concentrated inside the nucleus. Therefore, the HFB density has a smaller tail at large distances.

As we have already mentioned, in the present resonant continuum HF-BCS calculations we neglect all the continuum contribution except for the three low-lying resonances $d_{3/2}$, $g_{7/2}$, and $h_{11/2}$. This model space seems sufficient for a proper evaluation of pairing correlation energies up to the drip line. The rest of the continuum changes mainly the particle distribution. In order to get a particle density closer to the HFB results one needs to introduce in the resonant continuum HF-BCS calculations additional relevant pieces from the continuum. This work is in progress.

## V. CONCLUSIONS

In this paper we have discussed how one can actually solve the HFB equations with proper boundary conditions for the continuous spectrum and we have shown, for the case of neutron-rich Ni isotopes, how different treatments of the continuum can affect the pairing correlations. It was found that in the vicinity of the drip line pairing correlations are overestimated by the continuum discretization done in box HFB calculations. On the other hand, we have shown that the particle densities and the radii are rather insensitive to the way in which the continuum is treated in HFB calculations. This means that the quantities that are mainly related to the mean-field properties do not practically depend on the different treatments of continuum. We have also shown that the position of the two-neutron drip line is not affected by the way in which continuum is treated. This is due to the fact that the differences observed for the pairing correlations energies in the two HFB calculations are diminished when the two-neutron separation energies are calculated. Moreover, the two-neutron separation energies predicted by HF are not very different from the HFB results. This shows that these quantities are not indicated for testing the pairing correlations close to the drip line.

We have also analyzed how the exact HFB solutions compare to the resonant continuum HF-BCS approximation [9,10]. It was shown that the resonant HF-BCS calculations that include only the first three low-lying resonances provide a very good description of pairing correlation energies up to the drip line. On the other hand, in the vicinity of the drip line the radii predicted by the resonant continuum HF-BCS calculations are larger than the HFB radii and closer to the HF results. This shows that one should add to the first three low-lying resonances additional contributions of the continuum in order to evaluate better the particle densities for nuclei close to the drip line.

## ACKNOWLEDGMENTS

We thank J. Dobaczewski for providing us the code that solves the HFB equations with box boundary conditions. One of us (N.S.) would like to thank the Institute de Physique Nucléaire—Orsay for its hospitality. This work was done in the framework of IN2P3-IPNE Collaboration.

[1] S. T. Belyaev, A. V. Smirnov, S. V. Tolokonnikov, and S. A. Fayans, Yad. Fiz. **45**, 1263 (1987) [Sov. J. Nucl. Phys. **45**, 783 (1987)].
[2] A. Bulgac, preprint No. FT-194-1980, Institute of Atomic Physics, Bucharest, 1980, nucl-th/9907088.
[3] J. Dobaczewski, H. Flocard, and J. Treiner, Nucl. Phys. **A422**, 103 (1984).
[4] J. Dobaczewzki, W. Nazarewicz, T. R. Werner, J.-F. Berger, C. R. Chinn, and J. Dechargé, Phys. Rev. C **53**, 2809 (1996).
[5] J. Terasaki, P.-H. Heenen, H. Flocard, and P. Bonche, Nucl. Phys. **A600**, 371 (1996).
[6] S. A. Fayans, S. V. Tolokonnikov, and D. Zawischa, Phys. Lett. B **491**, 245 (2000).
[7] M. V. Stoitsov, W. Nazarewicz, and S. Pittel, Phys. Rev. C **58**, 2092 (1998).
[8] M. V. Stoitsov, J. Dobaczewski, P. Ring, and S. Pittel, Phys. Rev. C **61**, 034311 (2000).
[9] N. Sandulescu, R. J. Liotta, and R. Wyss, Phys. Lett. B **394**, 6 (1997).
[10] N. Sandulescu, N. Van Giai, and R. J. Liotta, Phys. Rev. C **61**, 061301(R) (2000).
[11] A. T. Kruppa, P. H. Heenen, and R. J. Liotta, Phys. Rev. C **63**, 044324 (2001).
[12] N. Sandulescu, O. Civitarese, and R. J. Liotta, Phys. Rev. C **61**, 044317 (2000).

[13] A. Bianchini, R. J. Liotta, and N. Sandulescu, Phys. Rev. C **63**, 024610 (2001).
[14] J. Meng, Phys. Rev. C **57**, 1229 (1998).
[15] M. Del Estal, M. Centelles, X. Viñas, and S. K. Patra, Phys. Rev. C **63**, 044321 (2001).
[16] K. Bennaceur (private communication).
[17] K. Bennaceur, J. Dobaczewski, and M. Ploszajczak, Phys. Lett. B **496**, 154 (2000).
[18] P. Möller *et al.*, At. Data Nucl. Data Tables **66**, 131 (1997).